Biochemistry and Biophysics Reports 42 (2025) 101963

Contents lists available at ScienceDirect

Biochemistry and Biophysics Reports

journal homepage: www.elsevier.com/locate/bbrep

The C-terminal end of PLIN1 displays structural disorder

Edgar D. Páez-Pérez [a,1], Miriam Livier Llamas-García [a,1], Gabriela M. Montero-Morán [b,**], Samuel Lara-González [a,*]

[a] IPICYT, Instituto Potosino de Investigación Científica y Tecnológica A.C., División de Biología Molecular, S.L.P, 78216, San Luis Potosí, Mexico
[b] Universidad Autónoma de San Luis Potosí, Facultad de Ciencias Químicas, S.L.P., 78216, San Luis Potosí, Mexico

ARTICLE INFO

Keywords:
Perilipin-1
PLIN1
Lipolysis
C-terminal end
Lipid droplets
Intrinsically disordered protein

ABSTRACT

Lipid droplets (LDs) serve as crucial organelles for lipid storage and metabolism, with their proteome significantly influencing their regulation. Perilipins (PLINs), in particular PLIN1, play vital role in LD metabolism by orchestrating lipolysis. The C-terminal end of PLIN1 regulates lipolysis through interactions with coactivators such as the CGI-58 protein. Despite its importance, the structural characterization of this domain remains limited. Here, we present a comprehensive bioinformatic and biophysical analysis of the C-terminal end of mouse PLIN1 (mPLIN1C). Our findings suggest that mPLIN1C behaves as an intrinsically disordered region (IDR), exhibiting context-dependent properties of the coil-like or pre-molten globule type. Structural analysis reveals a predominance of disordered secondary structure, with circular dichroism spectroscopy indicating a high coil content. Interaction studies with SDS micelles suggest a conformational transition towards a pre-molten globule state. Furthermore, the analysis of molecular recognition features (MoRFs) identifies the EPESE sequence spanning residues 413–417 as a potential binding site for partner molecules. Overall, our findings shed light on the structural properties and potential interaction mechanisms of mPLIN1C, providing insight into its functional role in LD metabolism.

1. Introduction

Lipid droplets (LDs) are ubiquitous organelles that store and supply lipids for energy metabolism, membrane synthesis and the production of lipid-derived signaling molecules [1]. While it is known that differences in the composition of the phospholipid monolayer or the neutral lipid core of LDs affect their metabolism and function, it is the proteome of these droplets that has emerged as a significant influencer in all aspects of LD biology [2]. Perilipins (PLINs) are a family of proteins that play a crucial role in lipid droplet metabolism and energy homeostasis. They are located on the surface of lipid droplets and act as scaffolds for other proteins, e.g. facilitating access for lipases, thus orchestrating lipolysis [3]. The perilipin family of proteins comprises several members that have been identified in human and mouse tissues, including perilipin 1 (PLIN1), perilipin 2 (PLIN2, also known as adipophilin or adipose differentiation-related protein), perilipin 3 (PLIN3, also known as TIP47), perilipin 4 (PLIN4), and perilipin 5 (PLIN5) [4]. The perilipin family was first defined based on their homology in the N-terminal PAT domain, which is present only in PLIN1, -2, -3 and -5 [5]. The PAT domain is followed by a region of 11-mer repeats of variable length, which is predicted to form amphipathic helices and is present in all five perilipins (PLIN1-5) [6]. Furthermore, it has been proposed that the carboxyl-terminal region of this family of proteins, contains a 4-helix bundle domain, which was initially identified in PLIN3 [7–9].

Among perilipins, PLIN1 is the most well-characterized protein. It plays a crucial role in the regulation of lipolysis and lipid metabolism. The protein is highly expressed in white adipocytes, where it increases triglyceride synthesis and promotes the formation of large LDs [10]. In comparison to the other PLINs, the C-terminal end of PLIN1 is distinctive, allowing it to regulate lipolysis. In the basal or fed state, the C-terminal end of PLIN1 sequesters the comparative gene identification 58 protein (CGI-58), an essential coactivator of adipose triglyceride lipase (ATGL), thereby preventing the activation of lipolysis. The release of CGI-58 is achieved through the phosphorylation of two serine residues located in the C-terminal region of PLIN1 (S492 and S517 of the mouse sequence), which is mediated by protein kinase A (PKA) in

* Corresponding author.IPICYT, Instituto Potosino de Investigación Científica y Tecnológica A.C., S.L.P., División de Biología Molecular, San Luis Potosí, Mexico.
** Corresponding author. Universidad Autónoma de San Luis Potosí, Facultad de Ciencias Químicas, S.L.P, San Luis Potosí, Mexico.
E-mail addresses: gabriela.montero@uaslp.mx (G.M. Montero-Morán), samuel.lara@ipicyt.edu.mx (S. Lara-González).
[1] These authors contributed equally to this work.

https://doi.org/10.1016/j.bbrep.2025.101963
Received 19 December 2024; Received in revised form 24 February 2025; Accepted 24 February 2025
Available online 28 February 2025

response to a β-adrenergic stimulus [11,12]. Once released, CGI-58 interacts with and activates ATGL, thereby initiating the hydrolysis of triglycerides stored in LDs [13]. It has been proposed that the region of interaction with CGI-58 spans residues 361 to 419 of PLIN1. This region is partially encoded in the unique C-terminal E9 exon of PLIN1, which initiates at residue 404. Therefore, this region differs significantly from other perilipins [13].

Lipolysis is a highly regulated process, in which PLIN1 has an important role to play, as patients with loss-of-function mutations in this protein have been found to exhibit elevated lipolysis, the metabolic consequences of which include partial lipodystrophy, severe insulin resistance, diabetes, dyslipidemia, and non-alcoholic fatty liver disease [14]. In a different context, it has been found that the expression of PLIN1 is significantly reduced in breast cancer samples, suggesting its potential as a disease marker. Diminished PLIN1 expression is particularly common in advanced tumors, and studies have demonstrated its ability to impede breast cancer cell proliferation, migration, and invasion [15]. Interestingly, PLIN1 haploinsufficiency has been linked to a favorable metabolic profile, including a reduction in the risk of cardiovascular disease, lower blood pressure, and a lower diagnosis of hypertension [16].

The structural characterization of full-length perilipins has not yet been achieved, largely due to the inherent challenges associated with the study of multi-domain peripheral membrane proteins. Furthermore, the currently available information on these proteins is largely limited to their individual domains. With regard to the C-terminal end of PLIN1, which plays a central role in the regulation of lipolysis, it has only been mentioned that it lacks a secondary structure. Many proteins, or regions within proteins, do not adopt stable secondary or tertiary structure under physiological conditions [17]. These intrinsically disordered proteins (IDPs) and intrinsically disordered regions (IDRs) exhibit remarkable functional versatility by mediating dynamic interactions with multiple binding partners [18]. They play crucial roles in regulation, signaling, and other cellular processes through high-specificity, low-affinity interactions that facilitate rapid assembly and disassembly of complexes. Moreover, their functions are frequently modulated by alternative splicing and post-translational modifications [19]. Although the involvement of IDPs/IDRs in lipid metabolism remains an area of active investigation [20], these regions are also implicated in processes such as signal transduction and transcriptional regulation [21,22]. Their inherent structural flexibility enables disorder-to-order transitions upon binding to targets, thereby integrating into complex regulatory networks. In this study, we present a bioinformatic and biophysical characterization of the C-terminal domain of the mouse PLIN1 protein. The results indicate that this domain behaves as an IDR of the coil-like type in solution, while in a lipid interaction model it adopts a pre-molten globule (PMG-like) conformation.

2. Materials and methods

2.1. Computational characterization of mPLIN1C

The amino acid sequence of mouse (NP_783571.2) and human (NP_001138783.1) PLIN1 protein, consisting of 517 and 522 residues respectively, were used for *in silico* analyses. The prediction profile of intrinsic disorder was generated using the VSL2 algorithm [23] as well as the hydrophobicity-hydrophilicity analyses [24,25], both available at http://www.pondr.com/. The charge-hydropathy analysis was conducted in accordance with the following procedure. For each protein sequence, the mean hydrophobicity was calculated using the Kyte-Doolittle scale by summing the hydrophobicity values of the individual amino acids and dividing by the total number of residues. The net charge per residue was calculated at pH 7.0 by adding the contributions of the ionizable residues based on their standard pKa values and then normalized by the length of the sequence. Subsequently, the average hydrophobicity (x axis) and the net charge (y axis) were plotted, and the boundary between ordered and disordered proteins was defined as recommended by Uversky et al. (Uversky, Gillespie & Fink, 2000). Amino acid composition was determined using Composition Profiler, available at http://www.cprofiler.org [26]. Secondary structure prediction was performed using Fast Estimator of Latent Local Structure (FELLS) (http://old.protein.bio.unipd.it/fells/) [27]. Molecular recognition features (MoRFs) prediction was carried out using the MoRFpred platform [28] (http://biomine.cs.vcu.edu/servers/MoRFpred/) and ANCHOR [29] (https://iupred2a.elte.hu/). The distribution of charged amino acids at the C-terminal end was calculated with the κ parameter using CIDER (https://pappulab.wustl.edu/CIDERinfo.html) [30].

2.2. Expression and purification of mPLIN1C

The cDNA encoding residues 406–517 of the mouse PLIN1 protein (mPLIN1C) was cloned between the *Nde*I and SaII restriction sites of the pET28 expression vector; this construct was designated pET28_mPLIN1C. The construct was transformed into competent cells of *Escherichia coli* BL21 (DE3) strain. The cells were grown at 37 °C until they reached an optical density at 600 nm of 0.6, at which point isopropyl-β-D-1-thiogalactopyranoside (IPTG) was added to a final concentration of 1 mM. The cells were then cultivated at the same temperature for an additional 4 h. The cells were harvested and resuspended in lysis buffer [50 mM Tris pH 8.0, 300 mM NaCl, 2 mM β-mercaptoethanol, and 10 mM imidazole] and sonicated on ice, followed by centrifugation at 12,000 rpm at 4 °C for 15 min. The supernatant of the lysed cells was loaded onto a column of Ni-NTA resin (Qiagen), which had been previously equilibrated with lysis buffer. The unbound protein fraction was washed with three column volumes of lysis buffer. A stepwise elution with imidazole (50, 250, and 500 mM) prepared in lysis buffer was applied to release the bound protein. Fractions containing the recombinant protein were collected and desalted in buffer A [50 mM HEPES pH 7.0, 300 mM NaCl, 2 mM β-mercaptoethanol, and 0.5 mM EDTA], then injected onto a Hitrap S HP column (GE Healthcare) that had been equilibrated with the same buffer. The protein was eluted by increasing the ionic strength with a linear gradient from 0.3 to 1 M NaCl with buffer B [50 mM HEPES pH 7.0, 300 mM NaCl, 2 mM β-mercaptoethanol, 0.5 mM EDTA, and 1 M NaCl]. The volume of the gradient was 75 mL. The protein concentration was measured at 205 nm (A_{205}) [31] using the calculated molar extinction coefficient $E^{0.1\,\%}_{205} = 30.79$ [32].

2.3. Analytical size-exclusion chromatography (SEC)

A purified sample of 100 μL of mPLIN1C at a concentration of 1 mg/mL was injected into a Superdex 75 10/300 GL column (GE Healthcare) equilibrated with SEC buffer [20 mM Tris-HCl pH 8.0, 150 mM NaCl, and 1 mM β-mercaptoethanol] at a flow rate of 0.5 mL/min at room temperature. The column was calibrated using the following standard proteins: ovalbumin (44 kDa), myoglobin (17 kDa), insulin (5.8 kDa), and vitamin B12 (1.35 kDa). The Stokes radii (R_S) of the standard proteins were calculated according to equation (1) [33].

$$\log(R_s) = -(0.204 \pm 0.023) + (0.357 \pm 0.005)\log(MW) \quad (1)$$

The total volume of the column (VT) was 24 mL, and the void volume of the column (V0) of 8.2 mL was determined using thyroglobulin. The elution volume (VE) of each standard protein was used to calculate the gel phase distribution coefficients (K_{AV} factors) according to equation (2) [34].

$$K_{AV} = \frac{V_E - V_0}{V_T - V_0} \quad (2)$$

2.4. Dynamic light scattering (DLS)

DLS experiments were conducted using a Zetasizer APS2000 instrument (Malvern Instruments) at 25 °C. The hydrodynamic radius (R_h)

of mPLIN1C was estimated at a concentration of 1 mg/mL in CD buffer [20 mM sodium phosphate pH 7.4 and 20 mM NaCl]. Protein denaturation was achieved by incubating it with increasing concentrations of urea overnight at room temperature. The R_h was measured for each urea concentration until complete protein unfolding was achieved. To determine the critical micelle concentration (CMC) of sodium dodecyl sulfate (SDS), the intensity of scattered light was measured in kilo counts per second (kcps) as a function of increasing SDS concentrations (0–5 mM) in CD buffer. The CMC value is determined by identifying the point of intersection between the line fitted to the data in the absence of micelles and the line of the data with micelles. The experiments were conducted in triplicate.

2.5. Circular dichroism spectroscopy (CD)

CD measurements were performed using a JASCO J-815 spectropolarimeter (Jasco Inc., Easton, MD) equipped with a Peltier temperature control system. The CD spectrum of mPLIN1C was recorded in the absence and presence of increasing concentrations of SDS (1–20 mM) over a wavelength range of 200–250 nm. To study protein unfolding, measurements were taken at a fixed wavelength of 222 nm over a temperature range of 20–90 °C. Ellipticity is reported as the mean ellipticity per residue [θ]. All samples were prepared at a protein concentration of 6 μM in CD buffer.

2.6. Differential scanning fluorimetry

The thermal stability of the protein was evaluated using a differential scanning fluorimetry (DSF) assay as previously described [35]. Samples were prepared at a final protein concentration of 0.5 mg/mL in 40 μL of a solution containing 50 mM HEPES pH 7.0, 0.1 mM EDTA, 5 mM β-mercaptoethanol, 450 mM NaCl, and 5X Sypro Orange (Invitrogen). Thermal denaturation of the protein was performed in a 7500 Fast RT-PCR instrument (Applied Biosystems) with a temperature gradient from 25 to 75 °C with 1 °C increments and 30 s incubation at each point. The excitation wavelength was 455–485 nm and the emission wavelength was 567–596 nm. Fluorescence readings from samples with protein were corrected by subtracting the signal from samples without protein. The melting curve was obtained by plotting the fluorescence intensities as a function of temperature. The data were fitted to the Boltzmann equation to calculate the thermal denaturation midpoint (T_m) according to Lee et al. [36].

3. Results and discussion

3.1. In silico analysis suggests the disordered nature of mPLIN1C

To date, there is little information on the PLIN protein family in the context of structural disorder. Among the early reports predicting the presence of intrinsic disorder, PLIN2 from the Pekin duck (*Anas platyrhynchos*) stands out, indicating that this protein has a short disordered region of 15 residues in its C-terminal domain [37]. Subsequently,

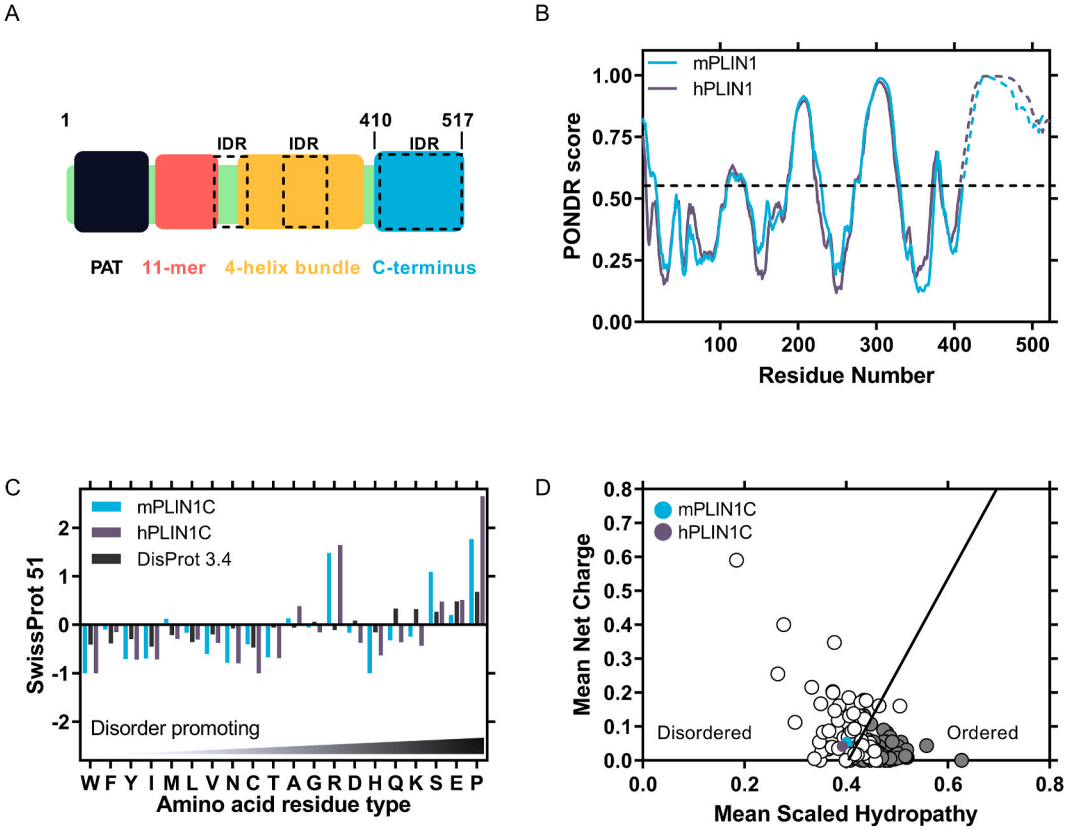

Fig. 1. *In silico* analysis of mPLIN1C. (A) Diagram representing the domain architecture of PLIN1. The N-terminal PAT domain (black), the 11-mer repeat region (red), and the 4-helix bundle domain (orange) of the PLIN family are shown together with the C-terminal domain (blue), which is distinctive of PLIN1. (B) Disorder prediction of mouse (blue) and human (purple) PLIN1 generated by the VSL2 algorithm of PONDR®; values above 0.5 indicate a high probability of disorder; The PLIN1C of each protein is marked with a dashed line. (C) Distribution of amino acids of mPLIN1C (blue) and hPLIN1C (purple) in relation to the SWISS-PROT database is shown; data are combined with the distribution of amino acids found in IDPs (black); enrichment (>0) or depletion (<0) in its composition was generated with Composition Profiler. (D) Hydropathy charge plot. Values of absolute average net charge versus average hydropathy for a set of disordered proteins (open circles) and ordered proteins (gray circles) were plotted together with mPLIN1C (blue) and hPLIN1C (purple).

predictions of disorder in the PLIN2 and PLIN3 proteins were documented in milk fat globules and it was proposed that disorder in these proteins plays an important role in their multifunctionality [38]. Recently, the presence of intrinsically disordered regions in the PAT domain and 11-mer repeats of PLIN3 was experimentally demonstrated using hydrogen-deuterium exchange mass spectrometry. Interestingly, these regions undergo a disorder-to-order transition when the protein interacts with the membrane [39].

With regard to PLIN1, the mouse protein (NP_001106942.1) consists of 517 amino acids whose domain distribution is shown in Fig. 1A. The N-terminal end of the protein contains the PAT domain (residues 1–93), which exhibits high conservation among members of the PLIN family. This is followed by the 11-mer repeat regions (residues 93–192) and the 4-helix bundle domain (residues 225–398). Recent findings have indicated that the 11-mer repeat regions are sufficient for LD binding, and that this interaction precedes the anchoring of the 4-helix bundle domain [8]. In comparison to other members of the family, the PLIN1 gene contains an additional exon E9, which begins at residue 406. Consequently, the C-terminus (residues 406–517) differs in size and length compared to other PLINs [13].

The mouse protein shares 82 % identity with the human protein (NP_001138783.1). However, this value decreases to 73 % when only their C-terminal ends are analyzed. Nonetheless, the disorder prediction profiles are very similar (Fig. 1B). This analysis allowed the identification of three regions with a high propensity to disorder that are common to both mPLIN1 and hPLIN1. Two of these within the 4-helix bundle (residues 185–229 and 272–330) and one in the C-terminal domain. In addition, a fourth region with a slightly lower propensity to disorder was found at the N-terminal end of mPLIN1 (residues 1–25), which was absent in hPLIN1. Given the significance of the C-terminal end in regulating lipolysis via the sequestration and release of CGI-58, we found it interesting that this distinctive region of PLIN1 was predicted to be disordered. Therefore, this sequence was subjected to further analysis.

The amino acid distribution of the aforementioned region was analyzed using the Composition Profiler web tool (Fig. 1C). The mouse C-terminal domain (mPLIN1C) showed a low proportion of order-promoting amino acids (W, F, Y, I, and N) compared to the SwissProt database. In contrast, this domain is enriched in disorder-promoting residues (R, S, and P) [40]. Therefore, the amino acid composition of mPLIN1C is similar to that of proteins deposited in the DisProt database [41], indicating that mPLIN1C exhibits characteristics of an intrinsically disordered region (IDR). In a similar manner, the amino acid composition of the C-terminal domain of the human protein (hPLIN1C) was consistent with those of IDPs. Further sequence analysis revealed that mPLIN1C and hPLIN1C have low mean hydropathy and high net charge (Fig. 1D). These properties are expected for IDPs [25]. Taken together, the disorder prediction results, the amino acid distribution analysis, and the low hydrophobicity/high net charge ratio collectively indicate that the C-terminus of PLIN1 should behave as an IDR in solution.

3.2. Expression and purification of mPLIN1C

To experimentally evaluate the predicted disordered nature of mPLIN1C, we expressed this domain in the *E. coli BL21* (DE3) strain. It should be noted that an attempt was also made to express and characterize the C-terminal end of the human protein. However, this was not feasible due to the low recombinant protein expression and purification challenges. The histidine-tagged protein was first purified on a nickel column. An additional purification step was performed by cation exchange chromatography to remove any remaining contaminants. Initial attempts to desalt the protein for column binding resulted in the formation of protein aggregates. Therefore, the protein was injected into the column at a salt concentration that prevented aggregation while enabling interaction with the column (300 mM NaCl). The protein was subsequently eluted at 350 mM sodium chloride. Further purification was not required, as the protein obtained so far showed the necessary purity. It is important to mention that the protein with the histidine tag was used for subsequent experiments, under the assumption that the tag does not affect the function or structure of mPLIN1C, as has been previously proposed [42,43].

The calculated theoretical molecular weight for the protein, including the His-Tag, was 15.6 kDa. However, mPLIN1C exhibited anomalous electrophoretic mobility, migrating at approximately 20 kDa (Fig. 2A). This was regarded as an initial indication of the protein's disordered behavior. As this is commonly observed in IDPs due to less efficient SDS binding compared to globular proteins of similar molecular weight, this is attributed to their unusual amino acid composition [44].

3.3. mPLIN1C has large hydrodynamic dimensions

SEC and DLS experiments were conducted to study the hydrodynamic properties of purified mPLIN1C, as these are useful parameters for estimating protein size and shape [45,46]. The hydrodynamic radius (R_h) is a parameter that allows disordered proteins to be distinguished from globular proteins, as it can take any value between the limits of the fully extended and fully collapsed states. Thus, it provides valuable insight into the conformational dynamics of IDPs in their environment [47].

In the analytical SEC assay, the protein eluted as a single peak (Fig. 2B) with an elution volume corresponding to a R_S of 28.3 Å (Fig. 2C). If we calculate the theoretical R_S for this domain, assuming a molecular weight of 15.6 kDa and a globular conformation, we obtain a value of 19.6 Å according to equation (1). The quotient of the radii results in an experimental value 1.4 times larger than the theoretical value. Therefore, the experimental volume (95 Å^3) and density (0.16 kDa/Å^3) values differ greatly from the calculated theoretical values of 31.5 Å^3 and 0.50 kDa/Å^3, respectively. The experimental value of R_S was compared with values determined for different folding states, including native, molten globule, pre-molten globule, native unfolded (coil-like), as well as guanidinium chloride unfolded (GdnHCl unfolded), by plotting the logarithm of the molecular weight against the logarithm of R_S [48,49]. As can be appreciated in Fig. 2D, the experimental R_S of mPLIN1C is situated between the pre-molten globule and coil-like conformations. These calculated hydrodynamic parameters indicate that mPLIN1C has larger dimensions compared to if it were a globular domain. This suggests that the protein is in an extended conformation or, alternatively, is forming an oligomer in solution.

To gain further insight into the molecular shape of this domain, we conducted DLS experiments to determine its hydrodynamic radius (R_h). The findings indicate that the domain adopts a coil-like structure with an R_h of 3.25 ± 1.15 nm (Fig. 3A), which approximates a molecular weight of 53.1 ± 10.4 kDa. The R_h value determined for mPLIN1C is in close agreement with the value that can be estimated for this protein in a fully extended conformation (R_h of 3.1 nm) [50]. Subsequently, a urea denaturation curve was performed to confirm that the broad size distribution is not reflecting domain oligomerization (Fig. 3B), since the theoretical molecular weight of the protein is 15.6 kDa. Therefore, if the domain were forming oligomers, an increase in urea concentration would result in a decrease in size, indicating monomer dissociation, which should have an estimated R_h of 1.9 nm (for a globular protein) [50]. Following this, the radius should reach approximately 3.1 nm until complete protein denaturation is achieved. However, our results showed that the R_h of mPLIN1C, both in the presence and absence of urea, is very similar to that of a denatured protein (unfolded), confirming the extended conformation of mPLIN1C. Oligomeric dissociation processes monitored by DLS have already been performed, for example, with the HbGp protein, which shows that pH changes to alkaline values promote dissociation [51]. The denaturation curve shows that as the urea concentration increases, the R_h remains constant, suggesting that no unfolding or oligomeric dissociation process is taking place. Therefore, it is suggested that the mPLIN1C domain is highly disordered in solution,

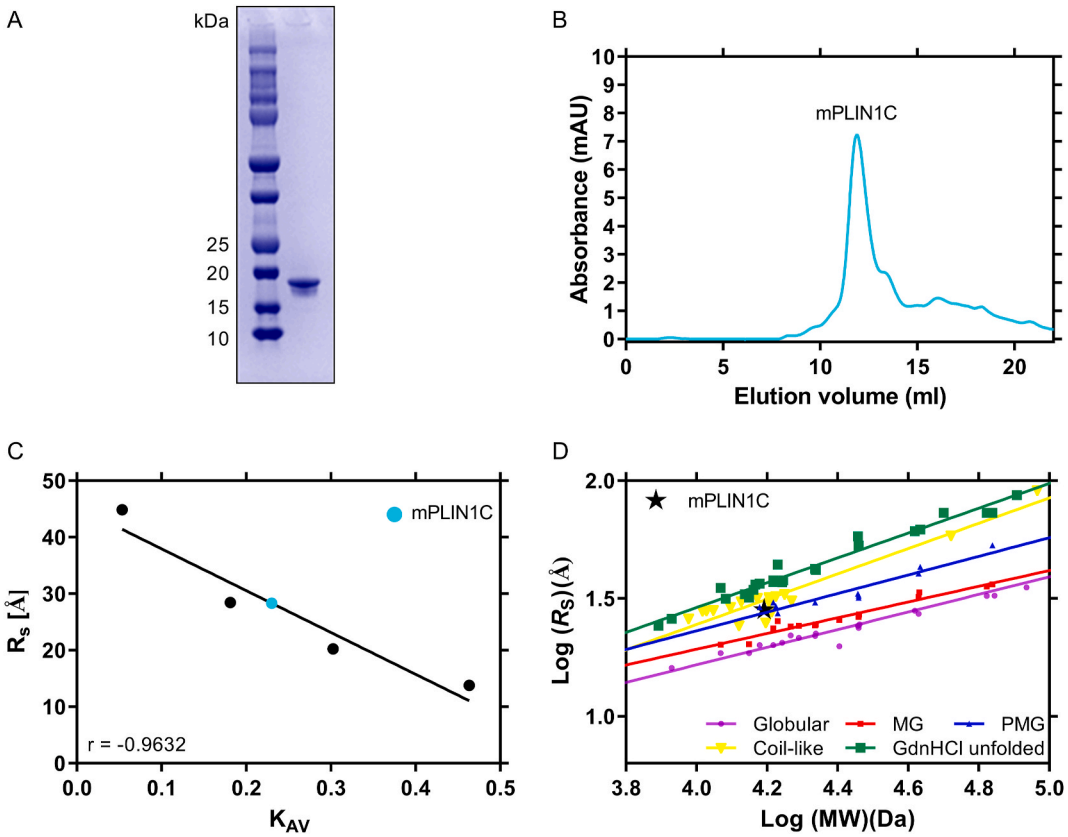

Fig. 2. Recombinant mPLIN1C exhibits hydrodynamic properties typical of intrinsically disordered proteins. (A) Electrophoretic profile of purified mPLIN1C. (B) Analytical SEC chromatogram; the blue curve represents the elution profile of mPLIN1C. (C) Calibration curve prepared by plotting the K_{AV} value of standard proteins (black points) versus their corresponding R_S value. The blue circle represents mPLIN1C. (D) Logarithmic graphs of the molecular weight (MW) versus the R_S for the indicated protein conformations. The position of mPLIN1C is indicated by the black star. The data for standard proteins used to plot the dependencies R_S (MW) were extracted from Ref. [48,49].

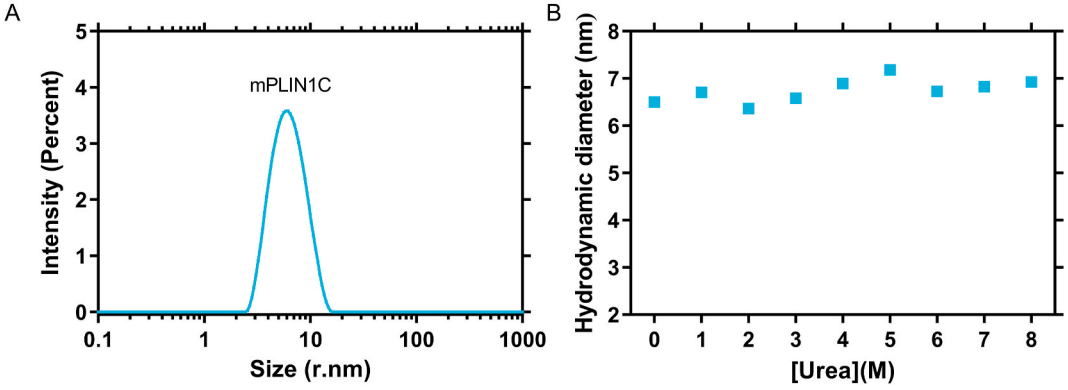

Fig. 3. Hydrodynamic radius of mPLIN1C in native and unfolded states. (A) Size distribution of mPLIN1C determined by DLS under native conditions. (B) Hydrodynamic radii of mPLIN1C determined by DLS under denaturing conditions. Protein samples were incubated overnight in the presence of increasing concentrations of urea before R_h determination.

as it has an extended conformation and no propensity for oligomerization. This is in line with the fact that IDPs lack a fixed spatial structure, which facilitates them to perform their regulatory functions and allows the efficiency of biochemical reactions to be controlled by temperature and the cellular environment [52].

3.4. The analysis of the secondary structure content indicates that mPLIN1C behaves as an intrinsically disordered protein

To obtain further information about the structure content of mPLIN1C, we employed far-ultraviolet circular dichroism spectroscopy [53]. The spectrum of mPLIN1C is consistent with that of a disordered protein, exhibiting negative ellipticity at 200 nm (−15167 deg·cm^2·dmol^{-1}) and low ellipticity at 222 nm (−1326 deg·cm^2·dmol^{-1}) (Fig. 4A). These features have been associated with the presence of residual secondary structure, estimated to be around 10–20 % [54]. Analysis of the CD data using the BestSel algorithm [55] indicates that mPLIN1C is predominantly disordered, showing a content of approximately ~54 % coil, ~26.3 % β-strands, ~19.7 % β-turns, and no contribution from α-helices (Table 1). The high coil content corroborates

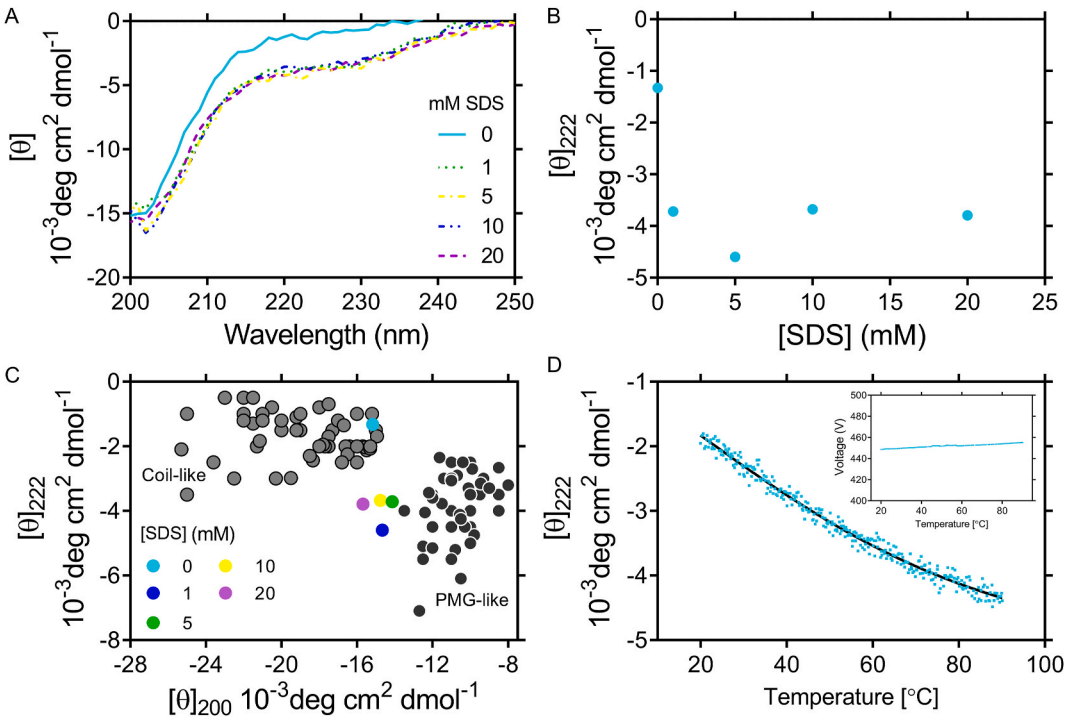

Fig. 4. Circular dichroism analysis of mPLIN1C. (A) CD spectra of mPLIN1C were recorded in buffer [20 mM sodium phosphate (pH 7.4) and 20 mM NaCl] at a protein concentration of 6 μM in the absence and presence of SDS. (B) Secondary structure gain in the presence of SDS. The relative amount of α-helicity was determined by measuring the molar ellipticity at 222 nm, with SDS concentrations varying from 1 to 20 mM. (C) A dual-wavelength plot showing [θ]222 versus [θ] 200 for coil-type (gray circles) and PMG-like (black circles); the position of mPLIN1C is indicated with a blue circle in the absence of SDS and with navy blue, green, yellow, and purple circles in the presence of increasing SDS concentration, respectively. (D) Molar ellipticity at 222 nm of mPLIN1C as a function of temperature. The temperature range used was 20–90 °C. The inset shows a graph of the dynode voltage throughout the entire scan.

the bioinformatics analysis, which also aligns with the domain having a high percentage (~42 %) of low-complexity regions in its sequence [56]. This is consistent with previous work indicating that this domain lacks secondary structure [13]. A detailed analysis using FELLS [27] reveals that the β-strands should comprise residues 408 to 414, 452 to 460, and 478 to 482. Furthermore, there are three additional segments with the potential to form a β-strand conformation, spanning residues 415 to 422, 467 to 476, and 488 to 497. The secondary structure content obtained by CD corresponds to the type of conformation this domain could have in solution. This prompted us to investigate what type of conformation this domain might adopt under conditions closer to native. To achieve this, we employed SDS micelles as a membrane model, as they have been considered as an appropriate substitute for mimicking the interactions that occur between proteins and lipids [57].

To determine the SDS concentration required to obtain micelles in the CD buffer, a DLS experiment was conducted, through which the critical micelle concentration (CMC) was estimated. DLS is suitable for studying micellization phenomena, as below the CMC, the detected scattered light intensity from each concentration is similar to that obtained from water, which in our case is the CD buffer. However, when the CMC is reached, the intensity of the scattered light increases due to the presence of micelles. From this point onwards, the intensity increases linearly as the number of micelles in the solution increases [58]. The CMC of SDS in the CD buffer was found to be 1.2 mM (Fig. 5). Subsequently, we acquired the CD spectrum in the presence of SDS micelles to detect any structural changes that this interaction might induce. In the presence of 1 mM SDS, we observed a shift in the CD

Table 1
Summary of the secondary structure content of mPLIN1C in the absence and presence of SDS.

Type of structure	[SDS] mM				
	0	1	5	10	20
Helix	0	6.2	5.9	3.1	1.6
Antiparallel	26.3	16.8	17.8	14.7	18.4
Parallel	0	0	0	0	0
Turn	19.7	20.2	17.9	19.3	18.1
Other (coil)	54	56.8	58.5	63	61.9
Total	100	100	100	100	100

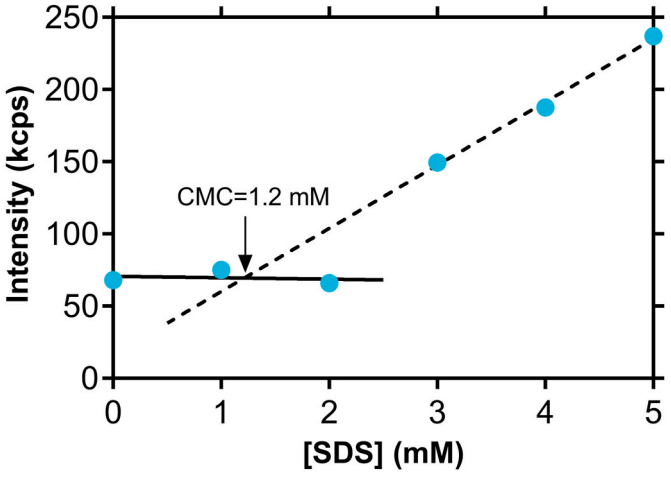

Fig. 5. Determination of the critical micelle concentration of SDS by dynamic light scattering. The scattered intensity (kcps) was plotted as a function of SDS concentration (mM). The solid line indicates the kcps in the absence of micelles, while the dashed line corresponds to the increase in scattered light resulting from the presence of micelles. The intersection of the two lines in the intensity data at 1.2 mM corresponds to the critical micellar concentration of SDS in CD buffer.

spectrum that remained constant as the concentration was increased up to 20 mM (Fig. 4A). There was a minimal change in the ellipticity observed at 200 nm, while a significant decrease in the CD signal was recorded at 222 nm (Fig. 4B). This indicates that in the presence of SDS micelles, mPLIN1C loses part of its β-conformation and gains α-helicity. However, there is also a slight increase in its coil structure, suggesting that it still maintains an extended conformation. A deeper analysis conducted by FELLS regarding the possible position of these formed α-helices indicates two regions comprising residues 423 to 432 and 507 to 514. These results show that a segment of mPLIN1C residues undergoes a transition from disordered to ordered in the presence of micelles. Similar results have been documented for residues 93 to 192 of PLIN1, encompassing the 11-mer domain, which also show a transition from disordered to ordered in the presence of micelles with α-helix formation [8]. It is important to note that the segment of residues acquiring α-helix structure at the C-terminus is shorter than that observed in the 11-mer domain. However, one of the segments identified by FELLS (507–514) is in close proximity to the phosphorylation site at position 517, which is critical for the interaction with CGI-58 [11,12]; therefore, the disorder-to-order transition of this region may be relevant for PLIN1 function.

The content of secondary structure has been used to classify IDPs into molten globule (MG), pre-molten globule (PMG), and random coil (RC) conformations. MG proteins have collapsed conformations with significant content of secondary structure; PMG proteins exhibit partially collapsed hydrophobic regions with residual secondary structure, while RC proteins have large hydrodynamic dimensions lacking secondary structure [59]. To determine the type of conformation present in the absence and presence of micelles, a dual-wavelength plot of ellipticity at 200 and 222 nm was analyzed (Fig. 4C). This approach has been used to differentiate IDPs into PMG and RC [49]. The data demonstrate that in the presence of micelles, mPLIN1C behaves like a PMG, which contrasts with our observations in solution, where the protein displayed a coil-like conformation. Therefore, the interaction with micelles promotes the stabilization of a partially collapsed structure.

On the other hand, it has been reported that intrinsically disordered proteins exhibit heat-induced folding. This is attributed to the increased hydrophobic effect that occurs at high temperatures, which is a major driving force in protein folding [60–62]. With this in mind, we analyzed the change in ellipticity at 222 nm with increasing temperature to identify a possible gain in structure. An increase in temperature globally resulted in a decrease in ellipticity at 222 nm (Fig. 4D), reaching a value of -4390 deg·cm^2·dmol^{-1} at a temperature of 90 °C. This value is similar to those obtained with micelles, suggesting that the formation of secondary structure is comparable for both types of induced folding.

In the present study, our characterization of mPLIN1C has thus far focused on two key aspects: the degree of compaction, which has been assessed using SEC and DLS, and the content of the secondary structure, which has been determined via far-UV CD. Differential scanning fluorimetry (DSF) has also been reported in the characterization of IDPs to infer tertiary structure content. This method, also known as Thermal Shift Assay, monitors the thermal unfolding of globular proteins using an environmentally sensitive fluorescent probe, that has negligible fluorescence in water but high fluorescence in a hydrophobic environment. By plotting fluorescence intensity against temperature, the protein's apparent melting temperature (T_m) is determined from the sigmoidal curve's inflection point. In contrast, IDPs show a flat, temperature-independent fluorescence profile, allowing them to be easily distinguished from structured proteins [44]. Therefore, we have set out to evaluate mPLIN1C using this technique. The DSF curve showed the typical behavior of an unfolded proteins (Fig. 6) [63]. At low temperatures, the sample displays elevated background fluorescence, which is consistent with the presence of exposed hydrophobic regions. However, at high temperatures, a flat profile was observed [64].

It has been noted that the conformational ensembles of IDPs are influenced by the net charge per residue [65]. Furthermore, the distribution of charged residues impacts the average size and shape of these proteins, as charge clustering leads to a restructuring of the conformational ensemble, promoting compaction [66].

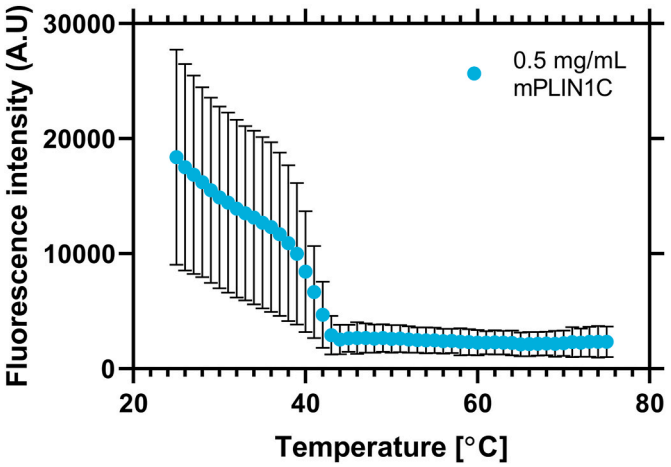

Fig. 6. Differential scanning fluorometry reveals the unfolded nature of mPLIN1C. Thermal denaturation curve of mPLIN1C in buffer [50 mM HEPES pH 7.0, 0.1 mM EDTA, 5 mM β-mercaptoethanol, 450 mM NaCl, and 5X Sypro Orange] is shown. Data shown are the mean and error bars represent the standard deviation (n = 3).

The amino acid composition indicates that mPLIN1C is enriched in arginine residues, and that the combination with lysine residues results in 20 positive charges (15 and 5 residues, respectively). This number is comparable to the 14 negative charges of aspartic and glutamic acid. Consequently, we aimed to assess whether these charges were evenly distributed or segregated, employing the κ parameter, along with their classification in the phase diagram of IDPs with the CIDER webserver [30]. The κ values vary between 0 and 1. A κ value of 0 indicates a uniform distribution of positive and negative charges throughout a linear sequence. Conversely, a κ value of 1 indicates the complete segregation of oppositely charged residues throughout the sequence [66]. The results indicate that mPLIN1C is located in region 2 of the phase diagram, with a κ value of 0.16. This is consistent with an extended conformation. A slight increase in segregation was observed for hPLIN1 compared to the mouse domain with a κ value of 0.2. However, it was also located in region 2 of the phase diagram (Fig. S1). Regarding region 2, it essentially serves as a boundary region that separates regions 1 and 3. Conformations within this region are likely to represent a continuum of possibilities between the types of conformations adopted by sequences in regions 1 (globules and tadpoles) and 3 (coils, hairpins, and chimeras) [67]. Therefore, we can have collapsed or expanded conformations, depending on the context, as suggested by the experimental data.

3.5. *Molecular recognition elements in mPLIN1C*

IDPs are highly dynamic and flexible, generally containing residual structural elements required for proper function [59]. In many cases, this flexibility allows IDPs to interact with multiple partners through direct molecular interaction. When IDPs bind to a target protein, DNA, or RNA and inhibit or activate the functions of the target, it is called an effector [59]. Previous studies have shown that these regions exhibit disorder-to-order transitions that facilitate interaction with multiple proteins [68]. Additionally, the exposure and flexibility of residues in IDPs are key factors facilitating post-translational modifications (PTMs) such as phosphorylation [69]. In this context, it has been demonstrated that under basal conditions, CGI-58 is the protein with which PLIN1 interacts, through its C-terminal end; however, with lipolysis stimulation, this domain undergoes phosphorylation for the complete release of

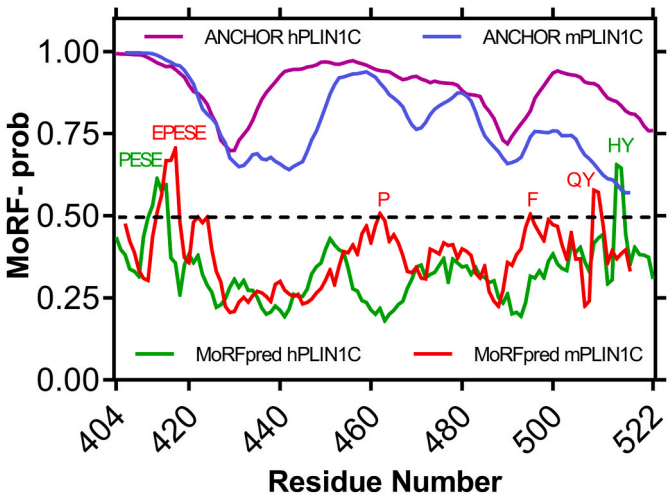

Fig. 7. Predicted molecular recognition features of mPLIN1C. (A) The results from MoRFpred and ANCHOR are shown in red and blue, respectively; the threshold value is 0.5. The putative MoRF with the highest probability corresponds to residues 413–417 (EPESE). Similar analyses were conducted for hPLIN1C, which revealed the same MoRF and comparable trends in both MorfPred (green) and ANCHOR (purple).

CGI-58.

Previous reports have indicated that the region involved in the interaction between PLIN1 and CGI-58 encompasses residues 382 to 429 of the C-terminal end of mouse PLIN1 [3]. Further reports indicate that the region of interaction with CGI-58 is located between residues 361 and 419 in the human sequence, which corresponds to residues 363 to 421 in the mouse sequence. Furthermore, it has been reported that the interaction is disrupted when the C-terminal end is deleted, beginning at position 1 of exon E9 (residue 404 in human or 406 in mouse). As previously stated, exon E9 is unique to PLIN1 and distinguishes it from the other family members [13]. This suggests that the interaction site at the mouse C-terminus is likely located between residues 406 and 421.

To gain insight into the potential interaction site, we analyzed the mPLIN1C sequence using the MoRFpred and ANCHOR servers to identify MoRFs with a propensity for disorder-to-order transitions. Both servers identified residues 413 to 417 (EPESE) as a MoRF region (Fig. 7). Interestingly, analyses of the human domain reveal a similar trend, with the only distinction being that the predicted MoRF is one residue shorter (PESE) than its mouse counterpart. Additionally, the FELLS server predicted that this segment has the potential to form an α-helix. These data suggest that the region encompassing the MoRF (EPESE) likely has the potential to interact with CGI-58, as it falls within the zone delimited by residues 406–421 and is exclusive to the C-terminal region absent in the other PLINs. Remarkably, a multiple sequence alignment of different species shows that the predicted interaction region is highly conserved, suggesting it performs an important biological function (Fig. S2). This emphasizes the necessity for additional research to elucidate the potential role of the presumed MoRF. In addition, it has been described that a single MoRF can bind to two or more different protein partners [70]. This may be the case for PLIN1, as recent evidence suggests that aquaglyceroporins also interact at the C-terminal end. This suggests that PLIN1 is involved in coordinating the subcellular translocation of aquaglyceroporins in human adipocytes [71].

4. Conclusion

This study provides a comprehensive bioinformatic and experimental characterization of the C-terminal domain of murine PLIN1. Bioinformatic analyses reveal its disordered nature, while experimental data confirm its dynamic structural features. These findings highlight the potential functional role of mPLIN1C in protein interactions and regulation. Future investigations will focus on the experimental analysis of the proposed MorRF sequence "EPESE" to further elucidate its biological relevance and activity. Specifically, these studies will explore how this sequence contributes to the structural functionality of mPLIN1C and its involvement in lipid metabolism and protein interactions.

CRediT authorship contribution statement

Edgar D. Páez-Pérez: Writing – original draft, Methodology, Investigation, Formal analysis, Conceptualization. **Miriam Livier Llamas-García:** Writing – review & editing, Methodology, Investigation, Conceptualization. **Gabriela M. Montero-Morán:** Writing – review & editing, Funding acquisition, Conceptualization. **Samuel Lara-González:** Writing – review & editing, Supervision, Project administration, Funding acquisition, Formal analysis, Conceptualization.

Declaration of competing interest

The authors declare that they have no known competing financial interests or personal relationships that could have appeared to influence the work reported in this paper.

Acknowledgments

This research was supported by the National Council of Science and Technology of Mexico (CONACyT) (grants CB-168710, A1-S-26028, and INFRA-204373). The authors, E.D. Páez-Pérez. and M.L. Llamas-García., would like to acknowledge the financial assistance provided by CONACyT through fellowships 453649 and 395867, respectively. We would also like to thank the Laboratorio Nacional de Biotecnología Agrícola, Médica y Ambiental (LANBAMA) for their technical support and access to their facilities.

Appendix A. Supplementary data

Supplementary data to this article can be found online at https://doi.org/10.1016/j.bbrep.2025.101963.

List of abbreviations

LD	Lipid Droplet(s)
PLIN	Perilipin(s)
PLIN1	Perilipin-1
IDR	Intrinsically Disordered Region
IDP	Intrinsically Disordered Protein
CGI-58	Comparative Gene Identification-58

(*continued on next page*)

(*continued*)

LD	Lipid Droplet(s)
ATGL	Adipose Triglyceride Lipase
SEC	Size-Exclusion Chromatography
CD	Circular Dichroism
DLS	Dynamic Light Scattering
CMC	Critical Micelle Concentration
DSF	Differential Scanning Fluorimetry
MoRF	Molecular Recognition Feature
FELLS	Fast Estimator of Latent Local Structure
CIDER	Classification of Intrinsically Disordered Ensemble Regions
GdnHCl	Guanidinium Chloride
MG	Molten Globule
PMG	Pre-Molten Globule
RC	Random Coil
R_S	Stokes Radius
R_h	Hydrodynamic Radius

Data availability

Data will be made available on request.

References

[1] T. Fujimoto, R.G. Parton, Not Just fat: the structure and function of the lipid droplet, Cold Spring Harbor Perspect. Biol. 3 (2011) 1–17, https://doi.org/10.1101/CSHPERSPECT.A004838.

[2] C.P. Najt, M. Devarajan, D.G. Mashek, Perilipins at a glance, J. Cell Sci. 135 (2022), https://doi.org/10.1242/JCS.259501/274665.

[3] D.L. Brasaemle, G. Dolios, L. Shapiro, R. Wang, Proteomic analysis of proteins associated with lipid droplets of basal and lipolytically stimulated 3T3-L1 adipocytes, J. Biol. Chem. 279 (2004) 46835–46842, https://doi.org/10.1074/JBC.M409340200.

[4] C. Sztalryd, D.L. Brasaemle, The perilipin family of lipid droplet proteins: gatekeepers of intracellular lipolysis, Biochim. Biophys. Acta 1862 (2017) 1221, https://doi.org/10.1016/J.BBALIP.2017.07.009.

[5] X. Lu, J. Gruia-Gray, N.G. Copeland, D.J. Gilbert, N.A. Jenkins, C. Londos, A. R. Kimmel, The murine perilipin gene: the lipid droplet-associated perilipins derive from tissue-specific, mRNA splice variants and define a gene family of ancient origin, Mamm. Genome : official journal of the International Mammalian Genome Society 12 (2001) 741–749, https://doi.org/10.1007/S00335-01-2055-5.

[6] A.R. Kimmel, D.L. Brasaemle, M. McAndrews-Hill, C. Sztalryd, C. Londos, Adoption of PERILIPIN as a unifying nomenclature for the mammalian PAT-family of intracellular lipid storage droplet proteins, Journal of lipid research 51 (2010) 468–471, https://doi.org/10.1194/JLR.R000034.

[7] S.J. Hickenbottom, A.R. Kimmel, C. Londos, J.H. Hurley, Structure of a lipid droplet protein: the PAT family member TIP47, Structure 12 (2004) 1199–1207, https://doi.org/10.1016/j.str.2004.04.021.

[8] E.R. Rowe, M.L. Mimmack, A.D. Barbosa, A. Haider, I. Isaac, M.M. Ouberai, A. R. Thiam, S. Patel, V. Saudek, S. Siniossoglou, D.B. Savage, Conserved amphipathic helices mediate lipid droplet targeting of perilipins 1-3, J. Biol. Chem. 291 (2016) 6664–6678, https://doi.org/10.1074/JBC.M115.691048.

[9] E. Griseti, A.A. Bello, E. Bieth, B. Sabbagh, J.S. Iacovoni, J. Bigay, H. Laurell, A. Čopič, Molecular mechanisms of perilipin protein function in lipid droplet metabolism, FEBS Lett. (2023), https://doi.org/10.1002/1873-3468.14792.

[10] L. Shijun, R. Khan, S.H.A. Raza, H. Jieyun, M. Chugang, N. Kaster, C. Gong, Z. Chunping, N.M. Schreurs, Z. Linsen, Function and characterization of the promoter region of perilipin 1 (PLIN1): roles of E2F1, PLAG1, C/EBPβ, and SMAD3 in bovine adipocytes, Genomics 112 (2020) 2400–2409, https://doi.org/10.1016/J.YGENO.2020.01.012.

[11] H. Miyoshi, J.W. Perfield, S.C. Souza, W.J. Shen, H.H. Zhang, Z.S. Stancheva, F. B. Kraemer, M.S. Obin, A.S. Greenberg, Control of adipose triglyceride lipase action by serine 517 of perilipin A globally regulates protein kinase A-stimulated lipolysis in adipocytes, J. Biol. Chem. 282 (2007) 996–1002, https://doi.org/10.1074/JBC.M605770200.

[12] J.G. Granneman, H.-P.H. Moore, R. Krishnamoorthy, M. Rathod, Perilipin controls lipolysis by regulating the interactions of AB-hydrolase containing 5 (Abhd5) and adipose triglyceride lipase (atgl) * □ S EXPERIMENTAL PROCEDURES generation of fluorescent fusion proteins and protein complementation constructs-construction and validation of fluorescently tagged proteins and bimolecular fluorescence, J. Biol. Chem. 284 (2009) 34538–34544, https://doi.org/10.1074/jbc.M109.068478.

[13] S. Patel, W. Yang, K. Kozusko, V. Saudek, D.B. Savage, Perilipins 2 and 3 lack a carboxy-terminal domain present in perilipin 1 involved in sequestering ABHD5 and suppressing basal lipolysis, Proceedings of the National Academy of Sciences of the United States of America 111 (2014) 9163–9168, https://doi.org/10.1073/PNAS.1318791111/SUPPL_FILE/PNAS.201318791SI.PDF.

[14] S. Gandotra, C. Le Dour, W. Bottomley, P. Cervera, P. Giral, Y. Reznik, G. Charpentier, M. Auclair, M. Delépine, I. Barroso, R.K. Semple, M. Lathrop, O. Lascols, J. Capeau, S. O'Rahilly, J. Magré, D.B. Savage, C. Vigouroux, Perilipin deficiency and autosomal dominant partial lipodystrophy, N. Engl. J. Med. 364 (2011) 740–748, https://doi.org/10.1056/NEJMOA1007487.

[15] C. Zhou, M. Wang, L. Zhou, Y. Zhang, W. Liu, W. Qin, R. He, Y. Lu, Y. Wang, X. Z. Chen, J. Tang, Prognostic significance of PLIN1 expression in human breast cancer, Oncotarget 7 (2016) 54488, https://doi.org/10.18632/ONCOTARGET.10239.

[16] K.A. Patel, S. Burman, T.W. Laver, A.T. Hattersley, T.M. Frayling, M.N. Weedon, PLIN1 haploinsufficiency causes a favorable metabolic profile, The Journal of Clinical Endocrinology & Metabolism 107 (2022) e2318–e2323, https://doi.org/10.1210/CLINEM/DGAC104.

[17] R. Trivedi, H.A. Nagarajaram, Intrinsically disordered proteins: an overview, Int. J. Mol. Sci. 23 (2022) 14050, https://doi.org/10.3390/ijms232214050.

[18] P.E. Wright, H.J. Dyson, Intrinsically disordered proteins in cellular signalling and regulation, Nat. Rev. Mol. Cell Biol. 16 (2015) 18–29, https://doi.org/10.1038/nrm3920.

[19] V.N. Uversky, C.J. Oldfield, A.K. Dunker, Intrinsically disordered proteins in human diseases: introducing the D 2 concept, Annu. Rev. Biophys. 37 (2008) 215–246, https://doi.org/10.1146/annurev.biophys.37.032807.125924.

[20] E. Deryusheva, E. Nemashkalova, M. Galloux, C.A. Richard, J.F. Eléouët, D. Kovacs, K. Van Belle, P. Tompa, V. Uversky, S. Permyakov, Does intrinsic disorder in proteins favor their interaction with lipids? Proteomics 19 (2019) https://doi.org/10.1002/PMIC.201800098.

[21] R. Nigam, M. Mohan, G. Shivange, P.K. Dewangan, R. Anindya, Escherichia coli AlkB interacts with single-stranded DNA binding protein SSB by an intrinsically disordered region of SSB, Mol. Biol. Rep. 45 (2018) 865–870, https://doi.org/10.1007/s11033-018-4232-6.

[22] M. Sztacho, J. Červenka, B. Šalovská, L. Antiga, P. Hoboth, P. Hozák, The RNA-dependent interactions of phosphatidylinositol 4,5-bisphosphate with intrinsically disordered proteins contribute to nuclear compartmentalization, PLoS Genet. 20 (2024) e1011462, https://doi.org/10.1371/JOURNAL.PGEN.1011462.

[23] K. Peng, P. Radivojac, S. Vucetic, A.K. Dunker, Z. Obradovic, Length-dependent prediction of protein intrinsic disorder, BMC Bioinf. 7 (2006) 208–212, https://doi.org/10.1186/1471-2105-7-208.

[24] V.N. Uversky, J.R. Gillespie, A.L. Fink, Why are "natively unfolded" proteins unstructured under physiologic conditions? Proteins 41 (2000) 415–427, https://doi.org/10.1002/1097-0134(20001115)41:3.

[25] V.N. Uversky, What does it mean to be natively unfolded? Eur. J. Biochem. 269 (2002) 2–12, https://doi.org/10.1046/J.0014-2956.2001.02649.X.

[26] V. Vacic, V.N. Uversky, A.K. Dunker, S. Lonardi, Composition Profiler: a tool for discovery and visualization of amino acid composition differences, BMC Bioinf. 8 (2007) 1–7, https://doi.org/10.1186/1471-2105-8-211/TABLES/1.

[27] D. Piovesan, I. Walsh, G. Minervini, S.C.E. Tosatto, FELLS: fast estimator of latent local structure, Bioinformatics 33 (2017) 1889–1891, https://doi.org/10.1093/BIOINFORMATICS/BTX085.

[28] F.M. Disfani, W.L. Hsu, M.J. Mizianty, C.J. Oldfield, B. Xue, A. Keith Dunker, V. N. Uversky, L. Kurgan, MoRFpred, a computational tool for sequence-based prediction and characterization of short disorder-to-order transitioning binding regions in proteins, Bioinformatics 28 (2012), https://doi.org/10.1093/BIOINFORMATICS/BTS209. Oxford, England.

[29] B. Mészáros, G. Erdös, Z. Dosztányi, IUPred2A: context-dependent prediction of protein disorder as a function of redox state and protein binding, Nucleic Acids Res. 46 (2018) W329–W337, https://doi.org/10.1093/NAR/GKY384.

[30] A.S. Holehouse, R.K. Das, J.N. Ahad, M.O.G. Richardson, R.V. Pappu, CIDER: resources to analyze sequence-ensemble relationships of intrinsically disordered proteins, Biophys. J. 112 (2017) 16–21, https://doi.org/10.1016/J.BPJ.2016.11.3200.

[31] R.K. Scopes, Measurement of protein by spectrophotometry at 205 nm, Anal. Biochem. 59 (1974) 277–282, https://doi.org/10.1016/0003-2697(74)90034-7.

[32] N.J. Anthis, G.M. Clore, Sequence-specific determination of protein and peptide concentrations by absorbance at 205 nm, Protein Sci. 22 (2013) 851–858, https://doi.org/10.1002/PRO.2253.
[33] S.E. Permyakov, I.S. Millett, S. Doniach, E.A. Permyakov, V.N. Uversky, Natively unfolded C-terminal domain of caldesmon remains substantially unstructured after the effective binding to calmodulin, Proteins: Struct., Funct., Bioinf. 53 (2003) 855, https://doi.org/10.1002/PROT.10481.
[34] P. Andrews, Estimation of molecular size and molecular weights of biological compounds by gel filtration, Methods of biochemical analysis 18 (1970) 1–53, https://doi.org/10.1002/9780470110362.CH1.
[35] M.L. Llamas-García, E.D. Páez-Pérez, C.G. Benitez-Cardoza, G.M. Montero-Morán, S. Lara-González, Improved stability of human CGI-58 induced by phosphomimetic S237E mutation, ACS Omega 7 (2022) 12643–12653, https://doi.org/10.1021/ACSOMEGA.1C06872/SUPPL_FILE/AO1C06872_SI_002.ZIP.
[36] P.H. Lee, X.X. Huang, B.T. Teh, L.M. Ng, TSA-CRAFT: a free software for automatic and robust thermal shift assay data analysis, SLAS discovery : advancing life sciences R & D 24 (2019) 606–612, https://doi.org/10.1177/2472555218823547.
[37] Y. Wu, X. Liu, S. Hou, H. Xiao, H. Zhang, Identification of adipose differentiation-related protein gene in Peking duck and its expression profile in various duck tissues, Mol. Biol. Rep. 38 (2011) 2479–2484, https://doi.org/10.1007/S11033-010-0384-8/FIGURES/3.
[38] E.M. Redwan, S.A. Alkarim, A.A. El-Hanafy, Y.M. Saad, H.A. Almehdar, V. N. Uversky, Disorder in milk proteins: adipophilin and TIP47, important constituents of the milk fat globule membrane, J. Biomol. Struct. Dyn. 38 (2020) 1214–1229, https://doi.org/10.1080/07391102.2019.1592027.
[39] Y.M. Choi, D. Ajjaji, K.D. Fleming, P.P. Borbat, M.L. Jenkins, B.E. Moeller, S. Fernando, S.R. Bhatia, J.H. Freed, J.E. Burke, A.R. Thiam, M.V. Airola, Structural insights into perilipin 3 membrane association in response to diacylglycerol accumulation, Nat. Commun. 14 (1 14) (2023) 1–16, https://doi.org/10.1038/s41467-023-38725-w, 2023.
[40] A.K. Dunker, J.D. Lawson, C.J. Brown, R.M. Williams, P. Romero, J.S. Oh, C. J. Oldfield, A.M. Campen, C.M. Ratliff, K.W. Hipps, J. Ausio, M.S. Nissen, R. Reeves, C.H. Kang, C.R. Kissinger, R.W. Bailey, M.D. Griswold, W. Chiu, E. C. Garner, Z. Obradovic, Intrinsically disordered protein, J. Mol. Graph. Model. 19 (2001) 26–59, https://doi.org/10.1016/S1093-3263(00)00138-8.
[41] M. Sickmeier, J.A. Hamilton, T. LeGall, V. Vacic, M.S. Cortese, A. Tantos, B. Szabo, P. Tompa, J. Chen, V.N. Uversky, Z. Obradovic, A.K. Dunker, DisProt: the database of disordered proteins, Nucleic Acids Res. 35 (2007) D786–D793, https://doi.org/10.1093/NAR/GKL893.
[42] M. Carson, D.H. Johnson, H. McDonald, C. Brouillette, L.J. DeLucas, His-tag Impact on Structure, vol. 63, 2007, pp. 295–301, https://doi.org/10.1107/S0907444906052024, *urn:issn:0907-4449*.
[43] S. Gräslund, P. Nordlund, J. Weigelt, B.M. Hallberg, J. Bray, O. Gileadi, S. Knapp, U. Oppermann, C. Arrowsmith, R. Hui, J. Ming, S. dhe-Paganon, H.W. Park, A. Savchenko, A. Yee, A. Edwards, R. Vincentelli, C. Cambillau, R. Kim, S.H. Kim, Z. Rao, Y. Shi, T.C. Terwilliger, C.Y. Kim, L.W. Hung, G.S. Waldo, Y. Peleg, S. Albeck, T. Unger, O. Dym, J. Prilusky, J.L. Sussman, R.C. Stevens, S.A. Lesley, I. A. Wilson, A. Joachimiak, F. Collart, I. Dementieva, M.I. Donnelly, W. H. Eschenfeldt, Y. Kim, L. Stols, R. Wu, M. Zhou, S.K. Burley, J.S. Emtage, J. M. Sauder, D. Thompson, K. Bain, J. Luz, T. Gheyi, F. Zhang, S. Atwell, S.C. Almo, J.B. Bonanno, A. Fiser, S. Swaminathan, F.W. Studier, M.R. Chance, A. Sali, T. B. Acton, R. Xiao, L. Zhao, L.C. Ma, J.F. Hunt, L. Tong, K. Cunningham, M. Inouye, S. Anderson, H. Janjua, R. Shastry, C.K. Ho, D. Wang, H. Wang, M. Jiang, G. T. Montelione, D.I. Stuart, R.J. Owens, S. Daenke, A. Schütz, U. Heinemann, S. Yokoyama, K. Büssow, K.C. Gunsalus, Protein production and purification, Nat. Methods 5 (2 5) (2008) 135–146, https://doi.org/10.1038/nmeth.f.202, 2008.
[44] A. Schramm, C. Bignon, S. Brocca, R. Grandori, C. Santambrogio, S. Longhi, An arsenal of methods for the experimental characterization of intrinsically disordered proteins – how to choose and combine them? Arch. Biochem. Biophys. 676 (2019) 108055 https://doi.org/10.1016/J.ABB.2019.07.020.
[45] K. Gast, C. Fiedler, Dynamic and static light scattering of intrinsically disordered proteins, Methods Mol. Biol. 896 (2012) 137–161, https://doi.org/10.1007/978-1-4614-3704-8_9.
[46] V.N. Uversky, Size-exclusion chromatography in structural analysis of intrinsically disordered proteins, Methods Mol. Biol. 896 (2012) 179–194, https://doi.org/10.1007/978-1-4614-3704-8_11/COVER.
[47] F. Pesce, E.A. Newcombe, P. Seiffert, E.E. Tranchant, J.G. Olsen, C.R. Grace, B. B. Kragelund, K. Lindorff-Larsen, Assessment of models for calculating the hydrodynamic radius of intrinsically disordered proteins, Biophys. J. 122 (2023) 310–321, https://doi.org/10.1016/J.BPJ.2022.12.013.
[48] O. Tcherkasskaya, V.N. Uversky, Denatured collapsed states in protein folding: example of apomyoglobin, Proteins: Struct., Funct., Bioinf. 44 (2001) 244–254, https://doi.org/10.1002/PROT.1089.
[49] V.N. Uversky, Natively unfolded proteins: a point where biology waits for physics, Protein Sci. 11 (2002) 739–756, https://doi.org/10.1110/PS.4210102.
[50] J.A. Marsh, J.D. Forman-Kay, Sequence determinants of compaction in intrinsically disordered proteins, Biophys. J. 98 (2010) 2374–2382, https://doi.org/10.1016/j.bpj.2010.02.012.
[51] P.S. Santiago, F. Moura, L.M. Moreira, M.M. Domingues, N.C. Santos, M. Tabak, Dynamic light scattering and optical absorption spectroscopy study of pH and temperature stabilities of the extracellular hemoglobin of glossoscolex paulistus, Biophys. J. 94 (2008) 2228–2240, https://doi.org/10.1529/biophysj.107.116780.
[52] M.K. Białobrzewski, B.P. Klepka, A. Michaś, M.K. Cieplak-Rotowska, Z. Staszałek, A. Niedźwiecka, Diversity of hydrodynamic radii of intrinsically disordered proteins, Eur. Biophys. J. 52 (6 52) (2023) 607–618, https://doi.org/10.1007/S00249-023-01683-8, 2023.
[53] N.J. Greenfield, Using circular dichroism spectra to estimate protein secondary structure, Nat. Protoc. 1 (6 1) (2007) 2876–2890, https://doi.org/10.1038/nprot.2006.202, 2007.
[54] P. Tompa, Intrinsically unstructured proteins, Trends Biochem. Sci. 27 (2002) 527–533, https://doi.org/10.1016/S0968-0004(02)02169-2.
[55] A. Micsonai, F. Wien, É. Bulyáki, J. Kun, É. Moussong, Y.H. Lee, Y. Goto, M. Réfrégiers, J. Kardos, BeStSel: a web server for accurate protein secondary structure prediction and fold recognition from the circular dichroism spectra, Nucleic Acids Res. 46 (2018) W315–W322, https://doi.org/10.1093/NAR/GKY497.
[56] P. Mier, L. Paladin, S. Tamana, S. Petrosian, B. Hajdu-Soltész, A. Urbanek, A. Gruca, D. Plewczynski, M. Grynberg, P. Bernadó, Z. Gáspári, C.A. Ouzounis, V. J. Promponas, A.V. Kajava, J.M. Hancock, S.C.E. Tosatto, Z. Dosztanyi, M. A. Andrade-Navarro, Disentangling the complexity of low complexity proteins, Briefings Bioinf. 21 (2020) 458–472, https://doi.org/10.1093/BIB/BBZ007.
[57] D.V. Tulumello, C.M. Deber, SDS micelles as a membrane-mimetic environment for transmembrane segments, Biochemistry 48 (2009) 12096–12103, https://doi.org/10.1021/BI9013819.
[58] Ö. Topel, B.A. Çakir, L. Budama, N. Hoda, Determination of critical micelle concentration of polybutadiene-block-poly(ethyleneoxide) diblock copolymer by fluorescence spectroscopy and dynamic light scattering, J. Mol. Liq. 177 (2013) 40–43, https://doi.org/10.1016/J.MOLLIQ.2012.10.013.
[59] J. Habchi, P. Tompa, S. Longhi, V.N. Uversky, Introducing protein intrinsic disorder, Chem. Rev. 114 (2014) 6561–6588, https://doi.org/10.1021/CR400514H/ASSET/CR400514H.FP.PNG_V03.
[60] X. Sun, W.T. Jones, D. Harvey, P.J.B. Edwards, S.M. Pascal, C. Kirk, T. Considine, D.J. Sheerin, J. Rakonjac, C.J. Oldfield, B. Xue, A.K. Dunker, V.N. Uversky, N-Terminal domains of DELLA proteins are intrinsically unstructured in the absence of interaction with GID1/gibberellic acid receptors, J. Biol. Chem. 285 (2010) 11557–11571, https://doi.org/10.1074/JBC.M109.027011.
[61] K. Hamdi, E. Salladini, D.P. O'Brien, S. Brier, A. Chenal, I. Yacoubi, S. Longhi, Structural disorder and induced folding within two cereal, ABA stress and ripening (ASR) proteins, Sci. Rep. 7 (2017), https://doi.org/10.1038/S41598-017-15299-4.
[62] M. Arai, Unified understanding of folding and binding mechanisms of globular and intrinsically disordered proteins, Biophysical Reviews 10 (2018) 163, https://doi.org/10.1007/S12551-017-0346-7.
[63] V. Velazhahan, P. Glaza, A.I. Herrera, O. Prakash, M. Zolkiewski, B.V. Geisbrecht, K. Schrick, Dietary flavonoid fisetin binds human SUMO1 and blocks sumoylation of p53, PLoS One 15 (2020) e0234468, https://doi.org/10.1371/JOURNAL.PONE.0234468.
[64] K. Gao, R. Oerlemans, M.R. Groves, Theory and applications of differential scanning fluorimetry in early-stage drug discovery, Biophysical Reviews 12 (1 12) (2020) 85–104, https://doi.org/10.1007/S12551-020-00619-2, 2020.
[65] A.H. Mao, S.L. Crick, A. Vitalis, C.L. Chicoine, R.V. Pappu, Net charge per residue modulates conformational ensembles of intrinsically disordered proteins, Proceedings of the National Academy of Sciences of the United States of America 107 (2010) 8183–8188, https://doi.org/10.1073/PNAS.0911107107/SUPPL_FILE/APPENDIX.PDF.
[66] G. Bianchi, M. Mangiagalli, A. Barbiroli, S. Longhi, R. Grandori, C. Santambrogio, S. Brocca, Distribution of charged residues affects the average size and shape of intrinsically disordered proteins, Biomolecules 12 (2022), https://doi.org/10.3390/BIOM12040561.
[67] R.K. Das, R.V. Pappu, Conformations of intrinsically disordered proteins are influenced by linear sequence distributions of oppositely charged residues, Proceedings of the National Academy of Sciences of the United States of America 110 (2013) 13392–13397, https://doi.org/10.1073/PNAS.1304749110/SUPPL_FILE/SAPP.PDF.
[68] P. Chakrabarti, D. Chakravarty, Intrinsically disordered proteins/regions and insight into their biomolecular interactions, Biophys. Chem. 283 (2022) 106769, https://doi.org/10.1016/J.BPC.2022.106769.
[69] E.A. Newcombe, E. Delaforge, R. Hartmann-Petersen, K. Skriver, B.B. Kragelund, How phosphorylation impacts intrinsically disordered proteins and their function, Essays Biochem. 66 (2022) 901–913, https://doi.org/10.1042/EBC20220060.
[70] W.L. Hsu, C.J. Oldfield, B. Xue, J. Meng, F. Huang, P. Romero, V.N. Uversky, A. K. Dunker, Exploring the binding diversity of intrinsically disordered proteins involved in one-to-many binding, Protein Sci. : A Publication of the Protein Society 22 (2012) 258, https://doi.org/10.1002/PRO.2207.
[71] P. Huang, J.S. Hansen, K.H. Saba, A. Bergman, F. Negoita, P. Gourdon, A. Hagström-Andersson, K. Lindkvist-Petersson, Aquaglyceroporins and orthodox aquaporins in human adipocytes, Biochim. Biophys. Acta Biomembr. 1864 (2022) 183795, https://doi.org/10.1016/J.BBAMEM.2021.183795.